Calibration and Evaluation of Parameters in A 3D Proximity Rotating Scanner

Ludek Zalud[1], Petra Kocmanova[2], Frantisek Burian[2], Tomas Jilek[2], Petr Kalvoda[3], Lukas Kopecny[2]
[1]*FNUSA ICRC, Brno University of Technology,*
Technicka 12, 616 00, Brno, Czech Republic
[2]*Central European Institute of Technology, Brno University of Technology,*
Technicka 12, 616 00, Brno, Czech Republic
[3]*Institude of Geodesy, Faculty of Civil Engineering, Brno University of Technology*
Veveri 331/95, 602 00, Brno, Czech Republic
zalud@feec.vutbr.cz

***Abstract*—This paper presents the procedures enabling the calibration and evaluation of intrinsic parameters in a Velodyne multi-beam laser scanner. As the device will be utilized in field robotics applications, both the evaluated parameters and the calibration are generally aimed to improve the performance of the scanner with advanced mapping algorithms such as robot evidence grids or octree. The measured parameters are compared with the data provided by the manufacturer. A novel calibration method based on conditional adjustment for correlated measurements is proposed and compared with factory calibration.**

***Index Terms*—Calibration, infrared sensors, multi-robot systems, data processing.**

I. INTRODUCTION

The reconnaissance of hazardous areas is one of the most challenging tasks for today's robotics. According to many indications, e.g. from the Robocup Rescue League community [1], the current development within the design of practical reconnaissance robots appears to be aimed at the following problems:

– Enabling a larger number of robots to be controlled by one operator, especially in cases when the operator must concentrate on vital tasks such as victim identification; in this type of situations, the robots are expected to perform the basic assignments (inclusive of mapping or self-localization) autonomously.

– Optimization of an easy and intuitive human-to-robot interface; the effort to solve this problem is based on the assumption that the real operators will not be specialists in robotics.

The robotics team at Brno University of Technology (BUT) intends to develop a heterogeneous robotic system [2], [3] for the reconnaissance of previously unknown, potentially dangerous, and/or contaminated environment.

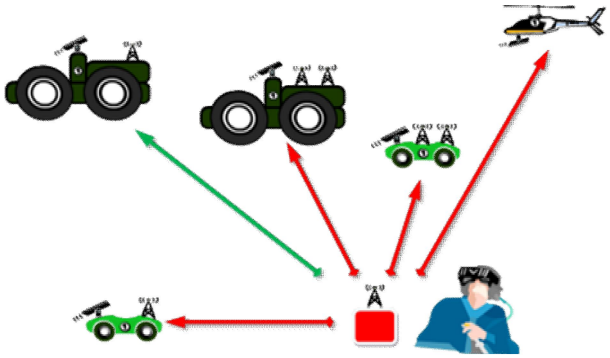

Fig. 1. Scheme of the CASSANDRA robotic system.

Although the technical features of individual robots are supposed to differ, the robots can be divided into certain "classes" of robots that are capable of being controlled with the control system. The classes are listed below with an emphasis on their mapping and self-localization abilities.

– Bigger and more complex robots with sufficient mapping and self-localization capabilities.

– Small robots with limited mapping and self-localization capabilities.

– Rotorcraft Unmanned Aerial Vehicles (UAVs) with self-localization only.

– Mapping robots with exceptional mapping and self-localization capabilities.

At present, the reconnaissance robots and the operator's telepresence control system, the CASSANDRA, are completed (Fig. 1 and Fig. 2, [4]); thus, each robot can be effectively controlled by the system, with help of visual telepresence and augmented reality [5]. The current task consists in enabling the automatic mapping and self-localization of the robots, and the first sub-task is to construct the mapping robot and formulate its precise mapping algorithms.

The present status of the robot being developed under the name EnvMap is shown in Fig. 3. The final design of the robot is not expected to be similar to the prototype, because the currently used drive configuration is unsuitable for hard terrain operation.

Manuscript received June 10, 2014; accepted November 19, 2014.

This work was supported by CEITEC – the Central European Institute of Technology (CZ.1.05/1.1.00/02.0068) utilizing the European Regional Development Fund, by the European Regional Development Fund - Project FNUSA-ICRC (No. CZ.1.05/1.1.00/02.0123), by the Technology Agency of the Czech Republic under the project TE01020197 "Centre for Applied Cybernetics 3", and by the project "EXCELLENT TEAMS" (CZ.1.07/2.3.00/30.0005) from European Social Fund.

a) b) c)

Fig. 2. Products designed by the BUT robotic group: a) the Orpheus-AC with an operator's station; b) the Scorpio; c) other robots based on the Cassandra system.

Fig. 3. The EnvMap robot with the Velodyne HDL-64E-S2 scanner.

Precise digital autonomous mapping of a previously unknown environment forms a crucial part of the entire robotic reconnaissance system. A typical activity requiring a faithful map of the environment is victim rescue planning, where the rescuers need to recognize the exact position of the victim, know the dimensions of the passages, and plan the victim-rescuer passage through the area.

The aim of this paper is to evaluate the intrinsic calibration parameters of the HDL-64E-S2 and HDL-32E 3D laser scanners and to propose a method facilitating an improvement in its original factory calibration. After such improvement, more accurate measurement could be performed to ensure precise mapping.

The calibration of laser scanners is commonly performed with respect to both intrinsic and extrinsic parameters. In intrinsic parameters, the calibration is based on comparing the scanner data with the real environment (mostly planar surfaces); after this initial phase, the subsequent estimation is carried out. The main tasks focused on the intrinsic parameters of a multi-beam LiDAR can be summarized as follows:

Muhammad and Lacroix, in [6], refine three intrinsic parameters (the correction of vertical angle, the correction of rotational angle, and the distance correction factor). For the calibration, the plane parallel to the X-Z plane of the scanner that was measured from different distances (10 m, 12 m, 14 m) is used.

In Atanacio-Jimenez *et al*. [7], the scanner is placed in the centre of a precisely made calibration object composed of 5 planes, and the intrinsic parameters are determined from the scan of the object. The intrinsic parameters are determined without using the factory-provided parameters.

Glenni and Lichti [8] utilize four walls of nearby buildings for the calibration. The configuration is changed by turning the scanner in the horizontal and vertical directions. The same authors analyse the temporal stability of a Velodyne scanner in [9]. In [10], a method for reducing the high correlation between the vertical angle correction and the vertical offset is proposed.

Mirzaei *et al*. [11] simultaneously calibrated the intrinsic and extrinsic parameters of an integrated Velodyne scanner and the Ladybug2 spherical camera system. The calibration plane was scanned from 40 different configurations.

Chen and Chien, in [12], designed a fully-automatic technique for determining the refined intrinsic parameters and proposed an alternative linear model for geometric interpretation. In [13], the same authors solved simultaneously the calibration of both intrinsic and extrinsic parameters. The checkerboard is observed by a scanner and 2 cameras under various positions, and in the computation it is used simultaneously with scene planes such as the walls, ceilings, and floors.

Levison, in [14], described an unsupervised extrinsic and intrinsic calibration method that does not require any calibration targets or manual measurement. This technique is applicable only for moving vehicles.

Two-step unsupervised calibration of only extrinsic parameters was solved by Zhu and Liu in [15]. Notably, all the above-mentioned papers deal with the calibration of a Velodyne HDL-64E multi-beam laser scanner; Chan *et al*. (in [10]) nevertheless analysed the calibration of a Velodyne HDL-32E scanner. In contrast with other calibration procedures indicated in our summary, the one applied by Chan et al. was based on the extraction of vertical cylinders from point clouds.

In this paper we propose calibration according to data exactly measured with close range photogrammetry, and such approach markedly differs from most other techniques, where the ground true data are merely estimated. The calibration is also performed for two types of scanners, namely the Velodyne HDL-64E and HDL-32E. We found only few resources presenting with the calibration of the HDL-32E.

II. THE VELODYNE HDL-64E AND HDL-32E SCANNERS

The Velodyne HDL-64E device is a high-speed 3D lidar which consists of 64 mounted lasers. Each laser is mounted at a specific vertical angle to a spinning head moving at a rate of 5 Hz to 15 Hz. The vertical field of view covers 26.8 degrees (from -24.8° down to +2° up). The Velodyne HDL-32E consists of 32 mounted lasers, and the vertical field of view covers 41.3 degrees (from -30.67° up to +10.67° up). The Cartesian coordinates of the 3D point are determined by the measured distance, the current rotational (horizontal) angle of the laser, the vertical rotational angle fixed for each laser, and correction parameters such as the vertical and horizontal offset. The distance standard error indicated in the datasheet of the Velodyne HDL-64E and HDL-32E is < 2 cm. [16], [17]

III. MEASUREMENT SETUP

The measurement interconnection diagram can be seen in

Fig. 4. The Velodyne laser scanner is connected directly to a notebook computer acting as a storage server for the measured data. Each packet collected from the scanner is stored to a measurement file; the structure of the stored packets is shown in Fig. 5.

Fig. 4. The EnvMap robot with the Velodyne HDL-32/64 scanner.

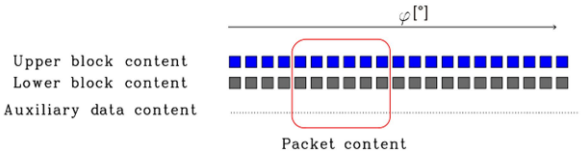

Fig. 5. Measurement file data structure.

Fig. 6. Processing data-flow.

The above shown image presents the basic structure of the UDP data stream from the laser scanner to the data storage. Three data streams are acquired from the sensor; two streams contain the measured distance data, and one auxiliary slower stream comprises the so-called auxiliary information about the current measurement conditions.

Each measurement block consists of 32 laser range and intensity measurements collected in each orientation of the sensor. The vertical composition of the upper and lower blocks (or the only one for HDL32) is interpreted as one full vertical measurement of the distance from the orientation.

By collecting six full measurements from six different orientations of the sensor (or 12 blocks with the data) with the some part of the stream, a 1248-byte packet is constructed. This packet is then sent through UDP port 2368 to the storage server. On the server, the packet data is concatenated into a stream and directly stored in the measurement file.

This method of storing raw data prevents the occurrence of any rounding and/or calculation-related errors in the data acquisition path; thus, unlike the approach described in [18], the technique applied within our research does not contain any communication-related redundant information, such as protocol headers and footers.

To process and analyse data, every 1248-byte packet buffer is sequentially read from the measurement file. After the reading process has finished, the packet is decomposed to measurement blocks, and these blocks are transformed to Cartesian space see Fig. 6.

IV. Mathematical Model of the Velodyne Scanner

The Cartesian coordinates of the 3D point are determined by the measured distance l, the current rotational angle φ of the laser i, and 5 correction parameters that are fixed for each laser. The scanner coordinate system is right-handed and orthogonal, and its origin lies in the centre of the base. An illustration of the directions of axes X, Y located in the plane of the bottom of the base is given in Fig. 7.

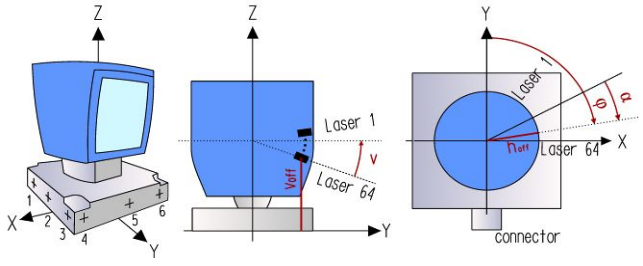

a) b) c)

Fig. 7. Frame of the Velodyne HDL64 scanner coordinates a); Parameters of the scanner in the vertical plane b); Parameters of the scanner in the horizontal plane c); for Velodyne HDL32 the alignment is analogous.

The following correction factors are used for the computation of the Cartesian coordinates:

– Rotational correction angle α, which denotes the angle between the laser beam and the Y-Z plane;

– Vertical correction angle v, which denotes the angle between the laser beam and the X-Y plane;

– Distance correction factor Δl, which denotes the value to be added to the distance returned by the corresponding laser;

– Vertical offset v_{off}; which denotes height of the laser from the bottom of the base;

– Horizontal offset h_{off}.

Definition of vertical offset is used according to the manufacturer [19], but some authors (for example [6], [7]) inappropriately used value of distance measured orthogonal to the laser beam, representing the distance of laser beam from origin in a vertical sense for vertical offset.

The distance $l_{X,Y}$ in the X, Y plane is calculated in the same manner as in [19]

$$l_{X,Y} = (l + \Delta l) \times \cos v. \tag{1}$$

The Cartesian coordinates X, Y, and Z according to [19] and if we consider rotational correction angle are calculated as follows:

$$\begin{cases} X = (l_{X,Y} \times \sin(¤ - \sim) - h_{off} \times \cos(¤ - \sim), \\ Y = (l_{X,Y} \times \cos(¤ - \sim) + h_{off} \times \sin(¤ - \sim), \\ Z = (l + \Delta l) \times \sin v + v_{off}. \end{cases} \tag{2}$$

By substituting (1) in (2), we have the following form:

$$\begin{cases} X = ((l + \Delta l) \cdot \cos v) \cdot \sin(¤ - \sim) - h_{off} \cdot \cos(¤ - \sim), \\ Y = ((l + \Delta l) \cdot \cos v) \cdot \cos(¤ - \sim) + h_{off} \cdot \sin(¤ - \sim), \\ Z = (l + \Delta l) \cdot \sin v + v_{off}. \end{cases} \tag{3}$$

Previous equation is valid for both types of scanners. But according to manufacturer [17], for Velodyne HDL32 only one correction factor is nonzero i.e. vertical correction angle.

V. Calibration Mathematical Model

The calibration process includes 3 stages. The first phase consists in the determination of transformation parameters

between two local orthogonal right-handed coordinate systems; the calculation of 6 congruence transformation parameters (3 translations, 3 rotations) is based on parametric adjustment Vanicek [20]. The second stage involves the computation of plane parameters, which is also based on parametric adjustment; the plane equation is obtained in the general form, where *a*, *b*, and *c* are the coefficients of the normal vector of the plane. The third stage comprises the determination of correction parameters; in the process, conditional adjustment for correlated measurements with heterogeneous variables is used. The condition consists in that the 3D point has to lie in plane with the known equation, i.e. the distance *s* from the measured point to the plane, in the given horizontal and vertical angles, should be zero. The distance d from the plane according to Koska et al. [21] is expressed by

$$d = \frac{a \times X + b \times Y + c \times Z - 1}{\sqrt{a^2 + b^2 + c^2}}. \tag{4}$$

The distance s in the given horizontal and vertical angles can be written as

$$s = \frac{a \times X + b \times Y + c \times Z - 1}{\sqrt{a^2 + b^2 + c^2} \times \cos|v| \times \sin}, \tag{5}$$

where β denotes the angle, whose calculation depends on the values of φ, ω (see Table I.). In the table, ω expresses the angle between the Y axis and the calibration plane.

Standard solution of this model is conditional adjustment with unknown's parameters. Distances l_i and rotational angles φ_i represent in this model direct observations and 5 correction factors Δl, α, v, v_{off}, h_{off} represent indirect observations. This adjustment model by Vanicek and Krakiwsky [22] has the following form. Transformed conditional equations are: $A\delta + Br + w = 0$, where *A*, *B* are design matrices, δ is vector of unknowns parameters corrections, *r* is residual vector , and *w* is misclosure vector:

$$A = \begin{pmatrix} \frac{\partial s_1}{\partial \Delta l} & \frac{\partial s_1}{\partial \sim} & \frac{\partial s_1}{\partial v} & \frac{\partial s_1}{\partial v_{off}} & \frac{\partial s_1}{\partial h_{off}} \\ \frac{\partial s_2}{\partial \Delta l} & \frac{\partial s_2}{\partial \sim} & \frac{\partial s_2}{\partial v} & \frac{\partial s_2}{\partial v_{off}} & \frac{\partial s_2}{\partial h_{off}} \\ \vdots & \vdots & \vdots & \vdots & \vdots \\ \frac{\partial s_n}{\partial \Delta l} & \frac{\partial s_n}{\partial \sim} & \frac{\partial s_n}{\partial v} & \frac{\partial s_n}{\partial v_{off}} & \frac{\partial s_n}{\partial h_{off}} \end{pmatrix}, \tag{6}$$

$$B = \begin{pmatrix} \frac{\partial s_1}{\partial l_1} & \frac{\partial s_1}{\partial \alpha_1} & 0 & 0 & & 0 & 0 \\ 0 & 0 & \frac{\partial s_2}{\partial l_2} & \frac{\partial s_2}{\partial \alpha_2} & & 0 & 0 \\ \vdots & \vdots & \vdots & \vdots & \ddots & \vdots & \vdots \\ 0 & 0 & 0 & 0 & & \frac{\partial s_n}{\partial l_n} & \frac{\partial s_n}{\partial \alpha_n} \end{pmatrix}. \tag{7}$$

If we need to determine less than all five correction parameters, the number of columns in the design matrix *A* will be the same as the number of determined parameters. The normal equations are written as:

$$\begin{bmatrix} M^{-1} & A \\ A^T & 0 \end{bmatrix} \begin{bmatrix} k \\ \delta \end{bmatrix} + \begin{bmatrix} w \\ 0 \end{bmatrix} = 0, \tag{8}$$

where *M* is the weight matrix of observation, and $k = M(A\delta + w)$ are the correlates. Vector of corrections δ is computed as $\delta = -N^{-1}u$, where $N = A^T MA$, and $u = A^T Mw$. Covariance matrix C_δ, from which we can compute standard errors of unknown parameters $\pm_{\delta_i} = \pm_0 \sqrt{C_{\delta_{ii}}}$, is $C_\delta = N^{-1}$ [22].

In the above described adjustment is disadvantageous that corrections are determined for indirect measurement δ (required for refinement of correction parameters) but also for direct measurements *r* (these correction are redundant and influence values of correction parameters).

TABLE I. CALCULATION OF ANGLE B.

	$\mu \in (0°,90°)$	$\mu \in (90°,180°)$
$\nu \in (0°,90°)$	$\nu - \mu$	$180° - (\pm - \mu)$
$\nu \in (90°,180°)$	$\nu - \mu$	$\mu - \nu$
$\nu \in (180°,270°)$	$(\nu - \mu) - 180°$	$\nu - \mu$
$\nu \in (270°,360°)$	$360° - (\nu - \mu)$	$180° - (\nu - \mu)$

New proposed adjustment model is going out from conditional adjustment [6]. Standard conditional adjustment isn't applicable, because number of conditional equations is greater than the number of redundant measurements. Condition equations have the form: $A^T\delta + w = 0$, where *A* is design matrix (same as in previous model), δ is vector of discrepancies, and *w* is vector of constant values. Normal equations are $AP^{-1}A^T k + w = 0$, where *P* is weight matrix, $k = -N^{-1}w$ are correlates, where $N = AP^{-1}A^T$. Discrepancies δ are computed as $\delta = P^{-1}A^T k$. To calculate N^{-1}, pseudoinversion [23]–[25] is used because the matrix *N* is rectangular and inversion for this matrix does not exist.

VI. TEST POINT FIELD

The test point field has been installed at the Department of Control and Instrumentation, Faculty of Electrical Engineering and Communication, BUT. The field consists of two matte planar vertical walls and floor (see Fig. 8). The walls dimensions are as follows: height 2 m, width 2.2 m and 5 m. The individual calibration steps are shown in Fig. 9. Before the actual measurement, two tasks related to functional configuration of the point field were performed. Firstly, it was necessary to establish whether the calibration planes are sufficiently flat to support the calibration; secondly, we fabricated the point field in a manner that enabled us to determine the origin of the scanner coordinate system and to specify the transformation parameters between the local coordinate system and the scanner coordinate system.

Fig. 8. The test point field.

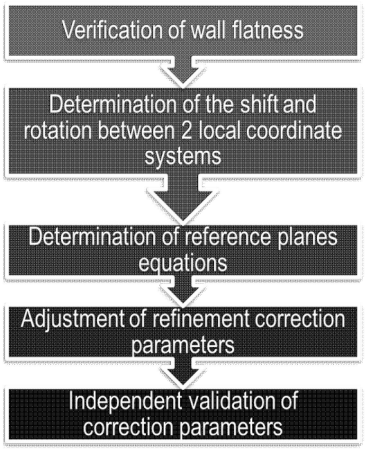

Fig. 9. Individual steps of Velodyne calibration.

Fig. 10. Individual steps of Velodyne calibration.

The point field measurement was realized using close range photogrammetry; the 23 ground control points were evaluated by the Topcon GPT 3003N total station, whose parameters are described in [26]. The coordinates were determined from the measured horizontal directions and vertical angles. Each ground control point was measured by no less than 3 positions of the total station, and the measurements were processed by means of a network adjustment method. The maximum coordinate mean square error of the ground control points was 0.89 mm; we stabilized the points by 8-bit coded targets (see Fig. 10). The stabilization of the remaining 372 points was performed via non-coded targets. To form these targets, we used black circles exhibiting the diameter of 50 mm. The circles were black laser prints on a white, matte self-adhesive foil. The coordinates of these points were determined by a photogrammetric method using the Canon EOS 7D digital single-lens reflex camera equipped with the Tokina 1224 mm–24 mm wide-angle lens. For this camera, we performed field calibration utilizing the 4-lens distortion parameter: *K1, K2* for the radial distortion, and *P1, P2* for the decentring distortion. The photogrammetric processing was executed in the PhotoModeler Scanner software by Eos Systems Inc.; to enhance the procedure, we also applied automatic target marking and referencing. The maximum coordinate mean square error detected in these points was 0.93 mm.

The general plane equation was calculated in the Matlab program; subsequently, we computed the deviations from the ideal plane of the two walls. In the shorter wall, the mean deviation is 1 mm and the maximum deviation 2 mm, while the values of the mean and maximum deviations established in the longer wall are 1 mm and 5 mm, respectively.

VII. Determination of the Origin and Specification of the Transformation Parameters

The determination of the transformation parameters can be performed only when there is a set of identical points in both systems. Consequently, six targets (3 on each side) were sticked to two sides of the scanner base, Fig. 7(a)), for the Velodyne HDL-64E; seven targets were utilized on the circular base of the Velodyne HDL-32E (angular spacing 30°). The first set of the scanner system coordinates in these points for the Velodyne HDL-64E was acquired from the measurement with a caliper. The distances between these six targets and structural elements of the scanner were measured; their relation to the origin is exactly given. For the Velodyne HDL-32E, it was not necessary to perform caliper measurements, because all targets are on the circumference of a cylinder; thus, the origin is exactly given as well.

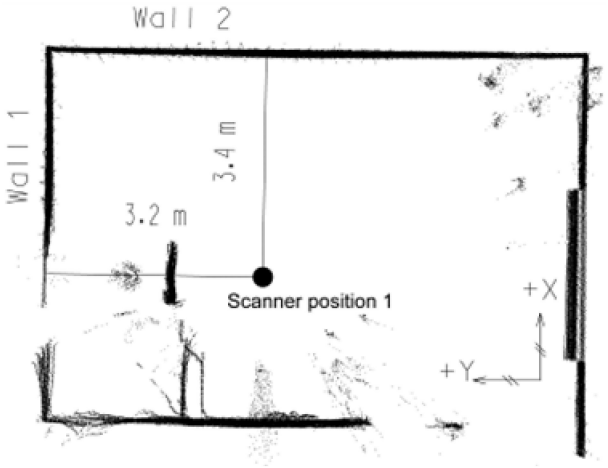

Fig. 11. Scanner position 1 – measured data in horizontal plane.

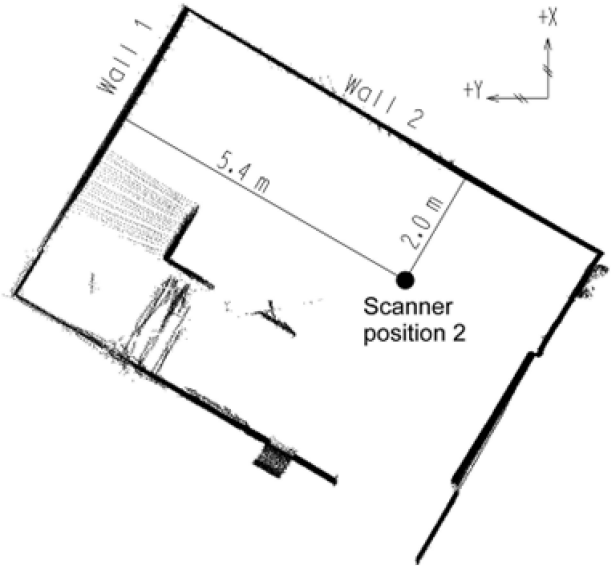

Fig. 12. Scanner position 2 – measured data in horizontal plane Correction parameters.

The maximum coordinate mean square error is 0.68 mm. The second set of local coordinates was established from the intersection of the directions. The related measurement was oriented to ground control points and performed using the Topcon GPT 3003N total station. The maximum coordinate mean square error for this set is 0.97 mm.

VIII. DATA COLLECTION

The dataset used for the Velodyne HDL-64E calibration comprised 4 samples (sa_1, sa_2, sa_3, sa_4) of the test point field. The data were collected from two scanner positions (floor projection of the situation is shown in Fig. 11 and Fig. 12) and under two different light conditions. In each position, we measured both with (sa_2, sa_3) and without (sa_1, sa_4) halogen light. Each measurement took 5 minutes. Three hundred rotations from each position/situation were chosen: 100 from the beginning, 100 from the middle, and 100 from the end of the measurement period. This approach enabled us to observe the influence of aspects such as rotation irregularity. The median of the measured distance for each rotational angle φ from each 100 rotations was calculated to accelerate the following computations.

For the Velodyne HDL-32E, only 2 samples (sa_5, sa_6) from two scanner positions were collected because we determined that various light conditions do not influence the values of the adjusted intrinsic parameters. Further processing was the same as in the previous case, namely that of the Velodyne HDL-64E.

IX. REFINEMENT OF THE CORRECTION PARAMETERS

The estimation for the Velodyne HDL-64E was performed starting from the default calibration data provided by the manufacturer. The refined correction parameters Δl, α, v were computed for scanner position 2 (sa_3, sa_4) and lasers 1-64. The correction parameters v_{off} and h_{off} were not determined again, because their corrections exhibit significantly smaller values than the distance standard error $\sigma = 2$ *cm*. Three sets of the refined correction parameters were determined: The first and the second sets as average values from the beginning, the middle, and the end of sa_3, sa_4, and the third one as a mean of the previous two.

In Table II, a comparison of the distance standard deviations is presented; therefore, the table contains a comparison of the distances s between the measured point and the plane in the given horizontal and vertical angle, before and after the calibration. The distance standard deviation is denoted as σ in the datasheet.

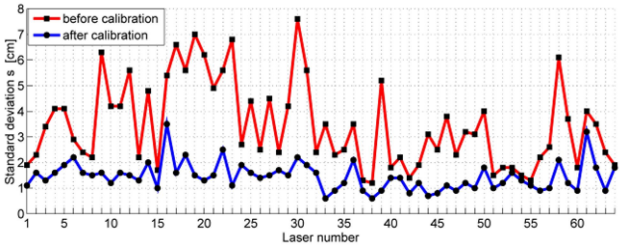

Fig. 13. Calibration Velodyne HDL-64E: distance standard deviation comparison between manufactory and our refined intrinsic parameters for each laser.

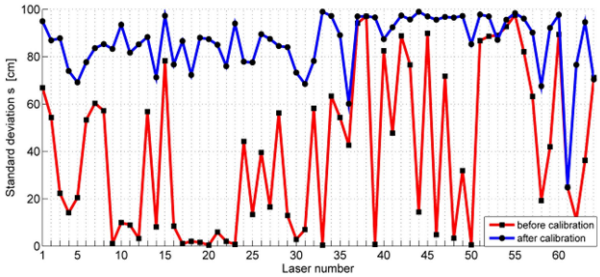

Fig. 14. Calibration Velodyne HDL-64E: percent of distance standard deviation smaller than 1 σ: for each laser before and after our calibration.

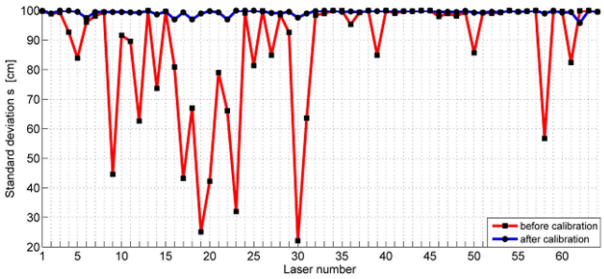

Fig. 15. Calibration Velodyne HDL-64E: percent of distance standard deviation smaller than 3 σ: for each laser before and after our calibration.

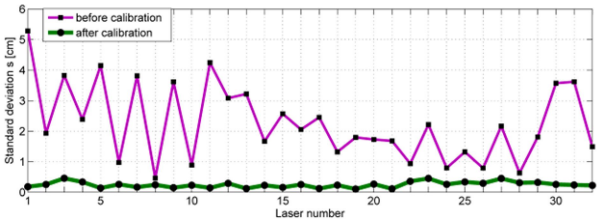

Fig. 16. Calibration Velodyne HDL-32E: distance standard deviation comparison between manufactory and our refined intrinsic parameters for each laser.

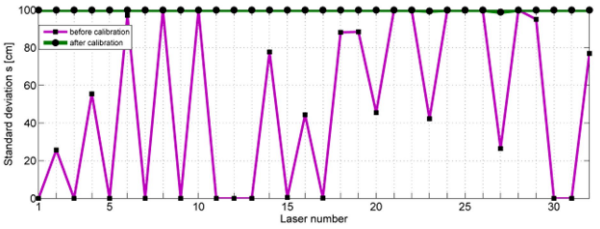

Fig. 17. Calibration Velodyne HDL-32E: percent of distance standard deviation smaller than 1 σ: for each laser before and after our calibration.

TABLE II. STANDARD DEVIATION S BEFORE AND AFTER THE CALIBRATION FOR VELODYNE HDL-64E.

	Before the calibration		
	Standard deviation [cm]	***s* to ± 1σ [%]**	***s* to ± 3σ [%]**
$sa_3^{beginnng}$	3.5	41.3	85.2
sa_3^{middle}	3.5	40.5	84.2
sa_3^{end}	3.4	40.8	87.7
$sa_4^{beginnng}$	3.3	38.1	89.3
sa_4^{middle}	3.3	37.9	90.1
sa_4^{end}	3.2	37.5	90.6
	After the calibration		
	Standard deviation [cm]	***s* to ± 1σ [%]**	***s* to ± 3σ [%]**
$sa_3^{beginnng}$	1.2	67.4	99,4
sa_3^{middle}	1.2	85.2	99,4
sa_3^{end}	1.2	89.7	99,5
$sa_4^{beginnng}$	1.2	90.3	99,5
sa_4^{middle}	1.2	89.4	99,4
sa_4^{end}	1.2	88.6	99,3

Figure 13 shows the distance standard deviation *s* for the scanner position 2 before and after the calibration. Figure 14 and Fig. 15 compare the percent of standard deviation *s* (smaller than 1σ, 3σ, respectively) before and after the calibration for 64 lasers. Illustration of the decreasing distance *s* for individual lasers 1 and 10 is shown in Fig. 18, Fig. 19.

Statistical testing of the achieved standard deviation was performed. In the test, the null hypothesis was that the variance of the data is greater than the squared standard deviation σ^2 (from [16]); by contrast, the alternative hypothesis assumed that the variance of the data is lower than the squared standard deviation σ^2. In the data before the calibration, the null hypothesis was rejected at the significance level of 5 % for 14 lasers; in the data after the calibration, the rejection applied to 51 lasers. We can therefore conclude that, after the calibration, 51 of the 64 lasers do not exhibit a standard deviation greater than that presented by the manufacturer.

TABLE III. STANDARD DEVIATION S BEFORE AND AFTER THE CALIBRATION FOR VELODYNE HDL-32E.

	Before the calibration		
	Standard deviation [cm]	***s* to ± 1σ [%]**	***s* to ± 3σ [%]**
$sa_5^{beginnng}$	2.3	49.0	100.0
sa_5^{middle}	2.3	49.1	100.0
sa_5^{end}	3.4	48.5	100.0
	After the calibration		
	Standard deviation [cm]	***s* to ± 1σ [%]**	***s* to ± 3σ [%]**
$sa_6^{beginnng}$	0.2	100.0	100.0
sa_6^{middle}	0.3	100.0	100.0
sa_6^{end}	0.2	99.9	100.0

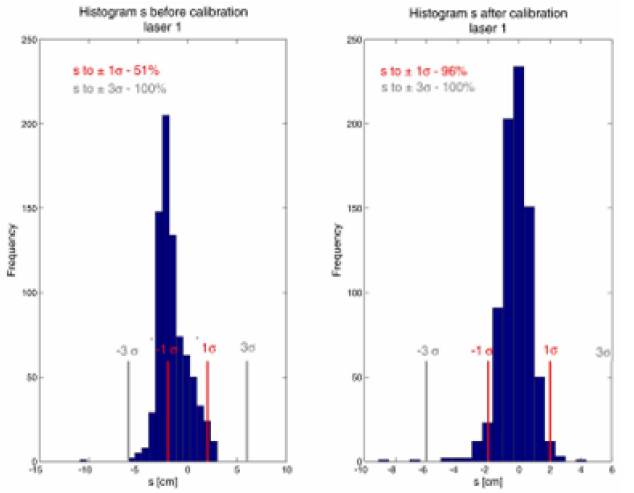

Fig. 18. Histogram of distance s for Velodyne HDL-64E laser 1 before and after the calibration.

The refined correction parameters for the Velodyne HDL-32E were computed for the scanner position 5. For the Velodyne HDL-32E, Fig. 16, Fig. 17 and Table IV are analogous to Fig. 13, Fig. 14 and Table II related to the Velodyne HDL-64E. The figure with comparison of the standard deviation smaller than 3σ is not shown, because before and after calibration all the values are approximately 100 %. Statistical testing of the achieved standard deviation was also performed. In the data before the calibration, the null hypothesis was rejected at the significance level of 5 % for 14 lasers; in the data after the calibration, the rejection applied to 32 lasers. We can therefore conclude that, after the calibration, all lasers of the Velodyne HDL-32E agree with the accuracy presented by the manufacturer.

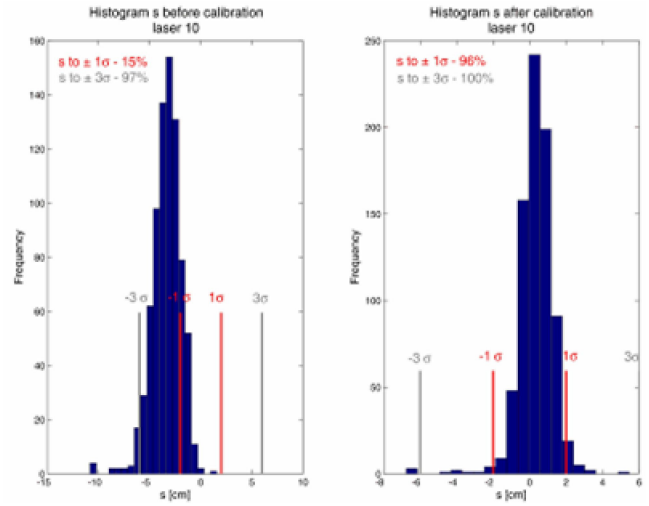

Fig. 19. Histogram of distance s for Velodyne HDL-64E laser 10 before and after the calibration.

X. INDOOR INDEPENDENT VALIDATION OF THE CORRECTION PARAMETER REFINEMENT

Independent validation of the three sets of the refined correction parameters was computed for the scanner positions 1 (sa_1, sa_2) and 6 (sa_6). From each sample, one scan was chosen from the beginning, the middle, and the end. The values *s* for the best fitting set of calibration parameters are shown in Table IV and V for the Velodyne HDL-64E and HDL-32E, respectively. Even though Table III and Table V include scanner positions 2 and 5, the scans indicated are different from those used in the calibration.

The standard deviation *s* using the refined correction parameters decreases approximately for Velodyne HDL-64E from 3.6 cm to 2.1 cm, and for Velodyne HDL-32E from 2.3 cm to 0.4 cm. The percentages of the standard deviations *s* that are related to the intervals ±σ, ±3σ is increased.

Figure 20–Fig. 24 show a comparison of the original and the refined correction parameters; the graphs display the percentage of the standard deviation *s* (smaller than 1σ, and 3σ, respectively) before and after the calibration for the 64 lasers in the Velodyne HDL-64E and the 32 lasers in the Velodyne HDL-32E. The figure with the standard deviation smaller than 3σ comparison for Velodyne HDL-32E is not shown, generally for the same reasons as in section refinement of the correction parameters.

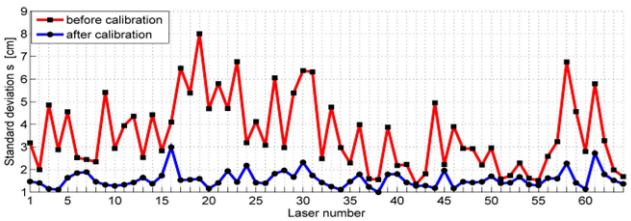

Fig. 20. Indoor independent validation of Velodyne HDL-64E: distance standard deviation comparison between manufactory and our refined intrinsic parameters for each laser.

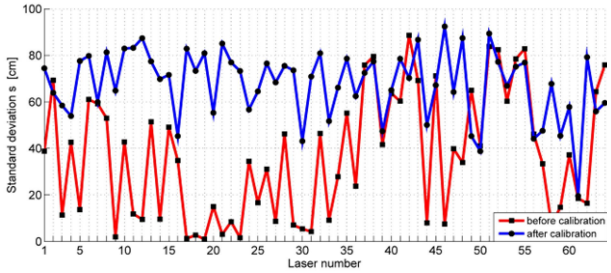

Fig. 21. Indoor independent validation of Velodyne HDL-64E: percent of distance standard deviation smaller than 1 σ: for each laser before and after our calibration.

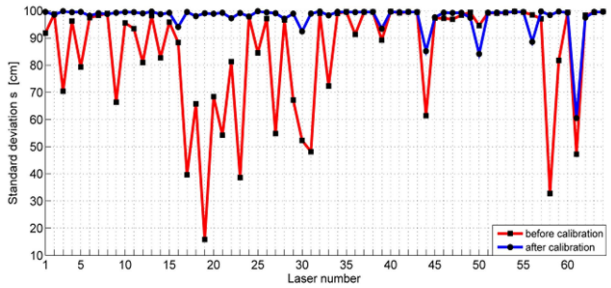

Fig. 22. Indoor independent validation of Velodyne HDL-64E: percent of distance standard deviation smaller than 3 σ: for each laser before and after our calibration.

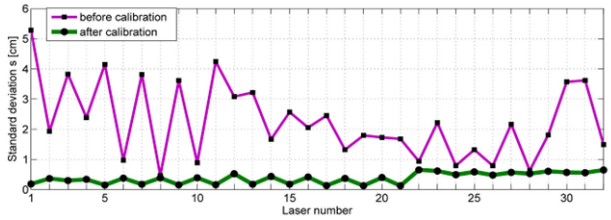

Fig. 23. Indoor independent validation of Velodyne HDL-32E: distance standard deviation comparison between manufactory and our refined intrinsic parameters for each laser.

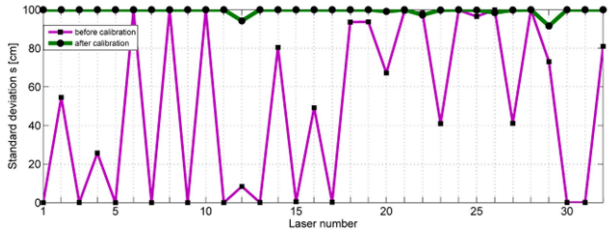

Fig. 24. Indoor independent validation of Velodyne HDL-32E: percent of distance standard deviation smaller than 1 σ: for each laser before and after our calibration.

TABLE IV. INDEPENDENT VALIDATION FOR VELODYNE HDL-64E: STANDARD DEVIATION S BEFORE AND AFTER THE CALIBRATION.

	Before the calibration		
	Standard deviation [cm]	***s* to ± 1σ [%]**	***s* to ± 3σ [%]**
$sa_1^{beginnng}$	3.6	35.6	85.5
sa_1^{middle}	3.6	35.8	85.3
sa_1^{end}	3.8	33.9	82.5
$sa_2^{beginnng}$	3.7	33.7	81.3
sa_2^{middle}	3.7	34.9	81.7
sa_2^{end}	3.7	35.5	82.1
$sa_3^{beginnng}$	3.6	39.8	83.1
sa_3^{middle}	3.6	40.2	83.9
sa_3^{end}	3.5	40.1	86.2
$sa_4^{beginnng}$	3.4	37.8	88.9
sa_4^{middle}	3.4	37.2	89.3
sa_4^{end}	3.3	37.1	89.7
	After the calibration		
	Standard deviation [cm]	***s* to ± 1σ [%]**	***s* to ± 3σ [%]**
$sa_1^{beginnng}$	2.1	66.6	98.0
sa_1^{middle}	2.5	52.9	97.2
sa_1^{end}	2.7	47.0	96.3
$sa_2^{beginnng}$	2.7	48.2	95.7
sa_2^{middle}	2.7	50.3	95.6
sa_2^{end}	2.7	51.4	95.3
$sa_3^{beginnng}$	1.9	73.0	98.9
sa_3^{middle}	1.6	82.8	99.0
sa_3^{end}	1.5	86.0	98.9
$sa_4^{beginnng}$	1.6	85.0	98.9
sa_4^{middle}	1.6	85.0	98.8
sa_4^{end}	1.7	83.9	98.8

Statistical testing of the achieved standard deviation was also performed for the independent validation. The null and alternative hypotheses were the same as those discussed in the previous section (H_0: the variance of the data is greater than the squared standard deviation σ^2↑H: the variance of the data is smaller than the squared standard deviation σ^2). For the Velodyne HDL-64E and the data with the original calibration parameters, the null hypotheses were rejected at the significance level 5 % for 14 lasers; for the data with the refined calibration parameters, the rejection applied to 36 lasers. The same test was carried out for the Velodyne HDL-32E. The null hypotheses for data with original calibration were rejected at the significance level 5 % for 14 lasers; for the data with the refined calibration parameters, the rejection applied to 32 lasers. It is therefore possible to conclude that, after the calibration all lasers do not exhibit a standard deviation greater than 2 cm.

TABLE V. INDEPENDENT VALIDATION FOR VELODYNE HDL-32E: STANDARD DEVIATION S BEFORE AND AFTER THE CALIBRATION.

	Before the calibration		
	Standard deviation [cm]	***s* to ±1σ [%]**	***s* to ±3σ [%]**
$sc_3^{beginnng}$	2.3	50.3	100.0
sa_3^{middle}	2.3	48.7	100.0
sa_3^{end}	2.3	47.9	100.0
$sa_4^{beginnng}$	2.3	52.6	100.0
sa_4^{middle}	2.3	50.4	100.0
sa_4^{end}	2.3	50.8	100.0
	After the calibration		
	Standard deviation [cm]	***s* to ±1σ [%]**	***s* to ±3σ [%]**
$sa_3^{beginnng}$	0.3	100.0	100.0
sa_3^{middle}	0.4	99.9	100.0
sa_3^{end}	0.4	99.6	100.0
$sa_4^{beginnng}$	0.4	99.2	100.0
sa_4^{middle}	0.4	98.6	100.0
sa_4^{end}	0.4	98.9	100.0

XI. OUTDOOR INDEPENDENT VALIDATION

Thus far we have performed indoor independent validation, and only distances of up to 6 m were evaluated. Another experiment nevertheless took place in outdoor locations, where we measured drywalls at distances ranging between 10 m and 35 m. The standard deviation of measured

distance for the Velodyne HDL-64E and computation with manufactory intrinsic parameters was 2.7 cm, and for refined intrinsic parameters with our calibration it was 1.9 cm. The detailed results are shown in Fig. 25.

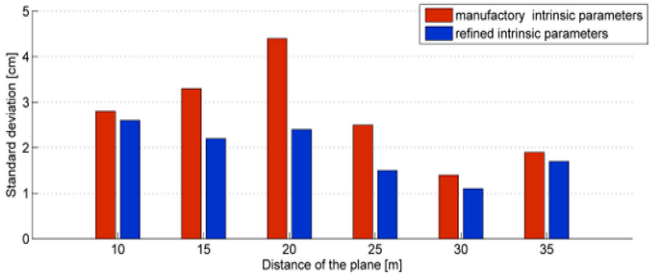

Fig. 25. Ideal condition outdoor independent validation for Velodyne HDL-64E: comparison of distance standard deviation for planes in different distances.

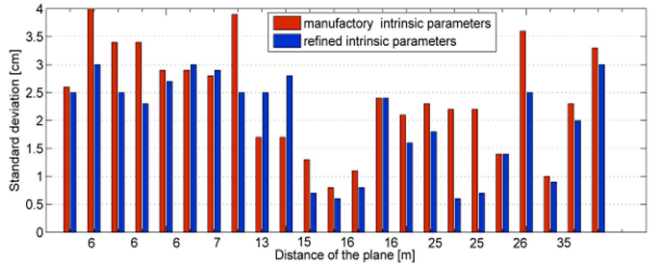

Fig. 26. Real condition outdoor independent validation for Velodyne HDL-64E: comparison of distance standard deviation for planes in different distances.

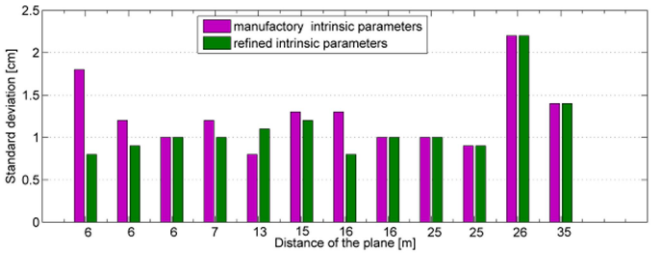

Fig. 27. Real condition outdoor independent validation for Velodyne HDL-32E: comparison of distance standard deviation for planes in different distances.

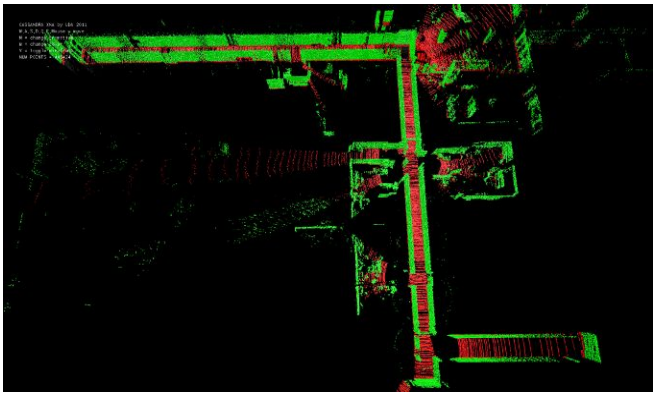

Fig. 28. The interior of a BUT building: A spatial map made by the Velodyne 3D lidar – 3D representation of more than 450000 points.

All previous experiments were performed in almost ideal conditions. We intended to verify the accuracy of the measurement under real conditions. The experiment was realized in front of the university premises, with a large number of students walking or moving around. The visibility was worsened by fog. At the edge of the pavement, two drywalls were placed; the robot with the scanner was driven along the sidewalk. We measured 15 samples with an approximate spacing of 10 meters for both devices, namely the Velodyne HDL-64E and the Velodyne HDL-32E. In Fig. 27, Fig. 28, the standard deviations of measured distances for various distances of the drywalls are shown. The standard deviation of measured distance for the Velodyne HDL-64E and computation with manufactory intrinsic parameters was 2.4 cm, and for refined intrinsic parameters 2.0 cm. The standard deviation for the Velodyne HDL-32E before our calibration was 1.3 cm, whereas with refined intrinsic parameters it decreased to 1.1 cm. In most cases, the standard deviation after calibration is smaller than before, except for distances of approximately 25 m; the manufacturer calibrates the scanners for this distance.

XII. CONCLUSIONS

As is apparent from the previous sections, the overall performance of the Velodyne HDL-64E and HDL-32E scanners do not entirely range within the limits defined by the manufacturer. According to our research, after the calibration of the Velodyne HDL-64E scanner only 36 from the 64 lasers comply with the parameters provided by the vendor. For the Velodyne HDL-32E, the number of lasers that satisfy the parameters provided by the manufacturer increased from 14 to 32 after our calibration. Although the manufacturer indicates the same accuracy for both these laser scanners, the results of our measurements show that the Velodyne HDL-32 is significantly more accurate than the HDL-64E. The performance of both scanners may be improved by using the proposed calibration method, which enabled us to reduce the standard deviation distance from 3.6 cm to 2.1 cm and from 1.3 cm to 1.1 cm in the Velodyne HDL-64E and HDL-32E, respectively.

In addition to the indoor-based calibration validation, we also performed outdoor validation under ideal and real conditions. Under ideal conditions, the Velodyne HDL-64E distance standard deviation for our refined intrinsic parameters was 30 % smaller than the value of intrinsic parameters provided by the manufacturer. For outdoor calibration under real conditions, the standard deviation distance from the measurement performed with our refined parameter is usually smaller – an average of 20 % for both scanners.

The presented evaluation experiments proved that the method ensures measurable enhancement of spatial data acquisition. In this context, it is necessary to point out that even though the calibration method itself is time-consuming and requires high computational power to acquire the parameters, the recalculation of the data is comparatively simple and fast; this characteristic is of vital importance for the planned mapping algorithms, which must work in real-time mode.

Preliminary results provided by our indoor mapping algorithms using an EnvMap robot and a Velodyne Lidar are shown in Fig. 28.

REFERENCES

[1] L. Zalud, “Orpheus - Universal reconnaissance teleoperated robot”, in *8th Int. RoboCup Symposium: Robot Soccer World Cup VIII (ROBOCUP 2004), Lecture Notes in Computer Science*, Germany,

2005, vol. 3276, pp. 491–498.

[2] L. Zalud, L. Kopecny, F. Burian, "Robotic Systems for Special Reconnaissance", in *Int. Conf. Military Technologies (ICMT 2010)*, Brno, Czech Republic, 2010, pp. 531–540.

[3] L. Nejdl, J. Kudr, K. Cihlarova, D. Chudobova, M. Zurek, L. Zalud, *et al.*, "Remote-controlled robotic platform ORPHEUS as a new tool for detection of bacteria in the environment", *Electrophoresis*, vol. 35, no. 16, pp. 2333–2345, 2014. [Online]. Available: http://dx.doi.org/10.1002/elps.201300576

[4] L. Zalud, L. Kopecny, F. Burian, "ORPHEUS Reconnissance Robots", in *IEEE Int. Workshop On Safety, Security & Rescue Robotics*, Sendai, Japan, 2008, pp. 31–34.

[5] L. Zalud, P. Kocmanova, F. Burian, T. Jilek, "Color and thermal image fusion for augmented reality in rescue robotics", in *8th Int. Conf. on Robotic, Vision, Signal Processing and Power Applications (RoViSP)*, Univ. Sains Malaysia, pp. 47–55.

[6] N. Muhammad, S. Lacroix, "Calibration of a rotating multi-beam lidar", in *IEEE/RSJ Int. Conf. Intelligent Robots and Systems (IROS)*, 2010, pp. 5648–5653.

[7] G. Atacio-Jimeenez, J. J. Gonzalez-Barbosa, J. B. Hurtado-Ramos, F. J. Ornelas-Rodriguez, H. Jimenez-Hernandez, T. Garcia-Ramirez, R. Gonzalez-Barbarosa, "LIDAR velodyne HDL-64E calibration using pattern planes", in *Int. Journal of Advanced Robotic Systems*, vol. 8, no. 5, pp.70–82, 2011.

[8] C. Glennie, D. D. Lichti, "Static calibration and analysis of the velodyne HDL-64E S2 for high accuracy mobile scanning", in *Remote Sensing*, vol. 2, pp. 1610–1624, 2010. [Online]. Available: http://dx.doi.org/10.3390/rs2061610

[9] C. Glennie, D. D. Lichti, "Temporal stability of the velodyne HDL-64E S2 scanner for high accuracy scanning applications", in *Remote Sensing*, vol. 3, pp. 539–553, 2011. [Online]. Available: http://dx.doi.org/10.3390/rs3030539

[10] T. O. Chan, D. D. Lichti, D. Belton, "Temporal analysis and automatic calibration of the velodyne HDL-32E LiDAR system", in *ISPRS Annals of the photogrammetry, remote sensing and spatial information sciences*, vol. 2, no. 5/W2, pp. 61–66, 2013.

[11] F. M. Mirzaei, D. G. Kottas, S. I. Roumeliotis, "3D lidar-camera intrinsic and extrinsic calibration: observability analysis and analytical least squares-based initialization", *Int. Journal of Robotics Research*, vol. 31, no. 4, pp. 452–467, 2012. [Online]. Available: http://dx.doi.org/10.1177/0278364911435689

[12] C.-Y. Chen, H.-J. Chien, "On-site sensor recalibration of a spinning multi-beam LiDAR system using automatically-detected planar targets", *Sensors*, vol. 12, pp. 13736–13752, 2012.

[13] C.-Y. Chen, H.-J. Chien, "Geometric calibration of a multi-layer LiDAR system and image sensors using plane-based implicit laser parameters for textured 3-D depth reconstruction", *J. Vis. Commun*. 2013. [Online]. Available: http://dx.doi.org/10.1016/j.jvcir.2013.08.005

[14] J. S. Levison, "Automatic laser calibration, mapping, and localization for autonomous vehicles", Ph.D. dissertation, Stanford University, 2011.

[15] Z. Zhu, J. Liu, "Unsupervised extrinsic parameters calibration for multi-bem LiDARs", in *Proc. 2nd Int. Conf. Computer Science and Electronics Engineering*, 2013, pp. 1110–1113.

[16] High Definition Lidar, Datasheet for Velodyne HDL-64E S2, Velodyne: Morgan Hill, CA, USA. [Online]. Available: http://velodynelidar.com/lidar/products/brochure/HDL-64E%20S2%20datasheet.pdf

[17] High Definition LidarTM, Datasheet for Velodyne HDL-32E, Velodyne: Morgan Hill, CA, USA. [Online]. Available: http://velodynelidar.com/lidar/hdldownloads/97-0038c%20HDL-32E%20datasheet_APR2012.pdf

[18] HDL-64E S2 and S2.1, User's manual and programming guide, Velodyne: Morgan Hill, CA, USA. [Online]. Available: http://velodynelidar.com/lidar/products/brochure/HDL-64E%20S2%20datasheet.pdf

[19] Diagram_correct.ppt, Velodyne: Morgan Hill, CA, USA. [Online]. Available: http://velodyne.com/lidar/doc/Documents/Doc%20Package/diagram_correct.ppt

[20] P. Vanicek, *Introduction to adjustment calculus*. Department of Geodesy & Geomatics Engineering University of New Brunswick: Fredericton, 1995.

[21] B. Koska, M. Stroner, J. Pospisil, "Algorithm of determination of the equation of the light plane for laser scanning", *Stavebni obzor*, vol. 12, no. 10, pp. 309–313, 2003.

[22] P. Vanicek, E. Krakiwsky, *Geodesy: The Concepts*. Amsterdam: Elsevier Science Publishers B. V., 1986.

[23] E. F. Galba, "Weighted pseudoinversion of matrices with singular weights", *Ukrainian Mathematical Journal*, vol. 46, pp. 1457–1462, 1994. [Online]. Available: http://dx.doi.org/10.1007/BF01066089

[24] I. V. Sergienko, E. F. Galba, V. S. Deineka, "Existence and uniqueness of weighted pseudoinverse matrices and weighted normal pseudosolutions with singular weights", *Ukrainian Mathematical Journal*, vol. 63, pp. 98–124, 2011. [Online]. Available: http://dx.doi.org/10.1007/s11253-011-0490-3

[25] A. Bjerhammar, *Theory of Errors and Generalized Matrix Inverses*. Amsterdam, 1973.

[26] Instruction Manual Pulse Total Station GPT-3000 Series, TOPCON CORPORATION 75-1 Hasunuma-cho, Itabashi-ku, Tokyo, Japan, pp. 174–8580. [Online]. Available: http://www.surveyequipment.com/PDFs/topcon-gpt-3000-manual.pdf